

Graphical Abstract

**Boundary-Refined Prototype Generation: A General End-to-End
Paradigm for Semi-Supervised Semantic Segmentation**

Junhao Dong, Zhu Meng, Delong Liu, Zhicheng Zhao, Fei Su

Highlights

Boundary-Refined Prototype Generation: A General End-to-End Paradigm for Semi-Supervised Semantic Segmentation

Junhao Dong, Zhu Meng, DeLong Liu, Zhicheng Zhao, Fei Su

- Research highlight 1
- Research highlight 2

Boundary-Refined Prototype Generation: A General End-to-End Paradigm for Semi-Supervised Semantic Segmentation

Junhao Dong^a, Zhu Meng^a, Delong Liu^a, Zhicheng Zhao^a, Fei Su^a

^a*School of Artificial Intelligence, Beijing University of Posts and Telecommunications, Beijing, 100876, China*

Abstract

Prototype-based classification is a classical method in machine learning, and recently it has achieved remarkable success in semi-supervised semantic segmentation. However, the current approach isolates the prototype initialization process from the main training framework, which appears to be unnecessary. Furthermore, while the direct use of K-Means algorithm for prototype generation has considered rich intra-class variance, it may not be the optimal solution for the classification task. To tackle these problems, we propose a novel boundary-refined prototype generation (BRPG) method, which is incorporated into the whole training framework. Specifically, our approach samples and clusters high- and low-confidence features separately based on a confidence threshold, aiming to generate prototypes closer to the class boundaries. Moreover, an adaptive prototype optimization strategy is introduced to make prototype augmentation for categories with scattered feature distributions. Extensive experiments on the PASCAL VOC 2012 and Cityscapes datasets demonstrate the superiority and scalability of the proposed method, outperforming the current state-of-the-art approaches. The code is available

at xxxxxxxxxxxxxxxxx.

Keywords:

Semantic segmentation, Semi-supervised learning, Prototype-based
contrastive learning, Mean teacher

1. Introduction

Semantic segmentation is an essential vision task, which finds extensive applications in real-world scenarios, e.g., autonomous driving [1, 2] and medical imaging [3]. In recent years, along with the advances in deep learning, rapid progress has been made in segmentation methods [4, 5, 6, 7]. Nevertheless, it requires large-scale dense pixel-level annotations, which are time-consuming and costly to obtain. To alleviate this problem, much research effort [8, 9, 10, 11, 12, 13, 14] has been dedicated to semi-supervised semantic segmentation, which aims to develop effective training pipelines with only limited annotations and numerous unlabeled data.

Early approaches to semi-supervised semantic segmentation mainly follow the scheme of adversarial learning with generative adversarial networks (GANs) [15, 16, 17]. In such a scheme, an additional discriminator is introduced to distinguish the segmentation maps (generated by the segmentation network) from the real ones (i.e., ground truth), thereby enhancing the prediction accuracy. Recently, more advanced methods have focused on the strategies of consistency regularization [13, 18, 19] and pseudo-labeling [20, 21, 22, 23]. The former involves applying perturbations at different levels (e.g., input, feature and network) to enforce the consistency of predictions, while the latter produces pseudo labels for unlabeled images to incorporate

them into the whole training pipeline. Both methods learn from unlabeled data in a pseudo-supervision manner.

In order to further explore unlabeled data, many powerful methods have introduced pixel-level contrastive learning [11, 14, 24, 25, 26] as an auxiliary task to augment supervision. Concretely, each pixel is mapped to a high-dimensional feature space, where the sampled instances are pulled towards their positive samples and pushed away from the negative ones. The positives can be the weakly augmented version of the same instances, or features belonging to the same category within the local context or the current batch, while the negatives are primarily sampled from different categories. Despite the optimization of inter-class separability can be achieved by contrastive learning, the issue of intra-class compactness is ignored, resulting in a scattered distribution of features within each class. Therefore, a prototype-based solution [27] is proposed, where each class is abstracted by a set of high-dimensional features, i.e., prototypes, to describe rich intra-class semantics. Specifically, pixels are pulled close to the positive prototypes associated with their respective classes and repelled from negative ones of other classes, which thereby facilitates the learning of compact representations.

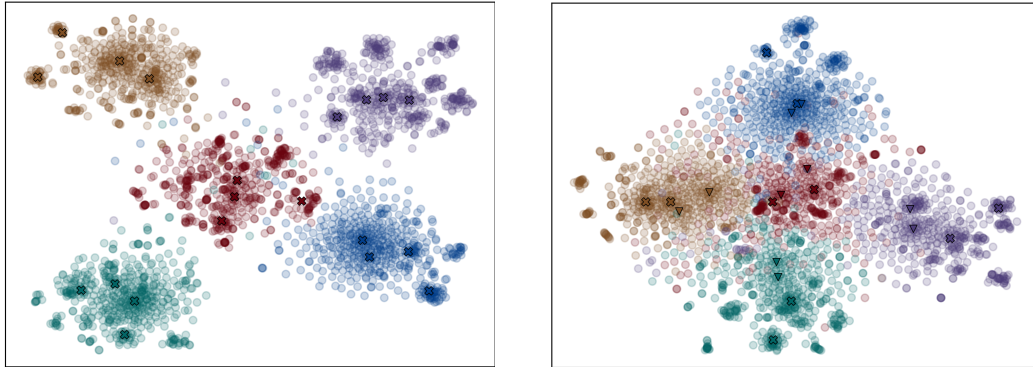
[28] represents the state-of-the-art method for prototype-based semi-supervised semantic segmentation, which can be divided into two stages. The first stage is prototype initialization. Specifically, a segmentation model is trained on labeled data with fully-supervised learning, allowing the extraction of feature representations. Subsequently, a certain number of features are randomly sampled to create K initial prototypes for each category using K -Means algorithm. In the second stage, a semi-supervised model is retrained, benefiting

from the initialized prototypes that are continuously updated throughout the training process.

However, this method prompts two critical questions: ① Given the abundance of redundant low-level semantics in the labeled images, is it necessary to separate the prototype initialization process from the semi-supervised training? ② Is there any better way to generate prototypes than this semantic-based one?

The answer to question ① is evidently negative. In this work, we propose an end-to-end prototype generation method, which can be integrated into the whole process of semi-supervised training. Specifically, apart from the inherent classification head, an additional feature extraction sub-net (a.k.a, feature head) is introduced to the segmentation model. During the sampling process, pixel-level features from both labeled and unlabeled data are simultaneously sampled to ensure feature alignment. We employ a category-wise memory bank to store these features, facilitating the generation of class prototypes with online K-Means clustering for subsequent training. It is worth noting that the feature head is not pretrained. Thus, the sampled features solely depend on the shared encoder and the well-designed structure of this sub-net. Intriguingly, the proposed approach achieves a comparable performance to [28] (76.77 vs. 77.16 on 366 split of PASCAL VOC 2012 Dataset [29]). This demonstrates that the randomly selected features during training can sufficiently capture the distribution of each category, obviating the need for a dedicated feature extractor trained on the entire dataset.

To answer question ②, it is important to clarify that prototype-based learning is essentially a nonparametric classification strategy based on the



(a) Random

(b) Confidence-based

Figure 1: Visualization of the feature embeddings sampled by two manners. (a) Random sampling and clustering. (b) Separate sampling and clustering based on a confidence threshold set as 0.8. “x” represents the generated prototypes in (a) and high-confidence prototypes in (b), while “v” denotes low-confidence prototypes, which tends to locate closer to the classification boundaries.

similarity between features and non-learnable prototypes. Hence, prototype initialization plays a crucial role in this task. Although the direct use of K-means for prototype generation has considered rich intra-class variance and exhibited strong semantics and interpretability, it may not be the optimal solution for the classification task. [30] is a GAN-based semi-supervised learning method. Theoretically, it has shown that generating low-quality samples helps the discriminator refine class boundaries in low-density regions, leading to an improvement of generalization performance. Inspired by this, we propose a simple approach to refine the classification boundaries through prototype generation. In particular, features of each class are divided into two groups with a confidence threshold to perform sampling and clustering respectively. It makes the low-confidence prototypes move closer

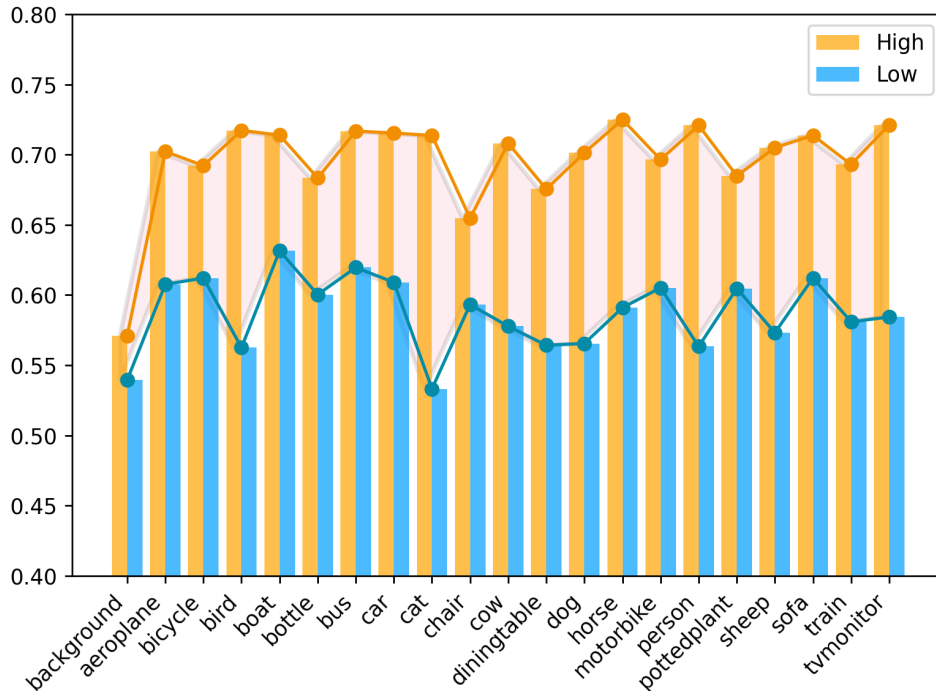


Figure 2: Mean cosine similarities between high- and low-confidence features with class centers on PASCAL VOC 2012 [29]. Lower values indicate features tend to deviate farther from class centers.

to the classification boundaries, capturing more difficult samples (as shown in Fig. 1). The statistical graph in Fig. 2 confirms that low-confidence features tend to deviate further from the category center, which also supports the viability of the proposed method. Moreover, an adaptive prototype optimization scheme is also applied, where we increase the number of generated prototypes for categories with scattered distributions.

Our method is implemented on the popular semi-supervised framework, Mean Teacher [31], with the specific training steps in Section 3. Experimental results on PASCAL VOC 2012 [29] and Cityscapes [32] datasets demon-

strate that it remarkably surpasses the existing prototype-based method [28], achieving state-of-the-art performance. Notably, the proposed method is also highly scalable, which can be easily incorporated into diverse semi-supervised frameworks. The successful integration with the classical framework FixMatch [33] serves as a compelling example, resulting in a significant enhancement over the baseline model. Our contributions can be summarized as follows:

1. We present a comprehensive end-to-end pipeline based on prototype learning for semi-supervised semantic segmentation. With online sampling and prototype generation, our approach remarkably outperforms the current prototype-based method.
2. The strategies of confidence-based prototype generation and adaptive prototype optimization are proposed to refine the initial classification boundaries, thereby enhancing the segmentation performance.
3. Our method achieves the state-of-the-art performance on benchmark datasets. Furthermore, the compatibility with FixMatch [33] confirms that our method is a general plug-and-play approach.

2. Related work

2.1. Semi-Supervised Learning

Semi-supervised learning (SSL) [34] has been widely applied to the scenarios where labeled data is limited but a large number of unlabeled data can be acquired. The key to success is how to effectively utilize the latent supervision in unlabeled data. Existing methods primarily belong to two representative families: consistency regularization [31, 35, 36, 37, 38, 39] and

entropy minimization [33, 40, 41, 42]. Consistency regularization methods, derived from the smoothness assumption, aim to encourage the network to produce consistent predictions on the same example under different augmentations. For example, MixMatch [36] and VAT [39] apply perturbations at the input and feature levels individually to regularize the outputs of the network. While Mean Teacher [31] incorporates an additional weight-averaged network to regularize the prediction consistency. Entropy minimization focuses on the implementation of self-training with generated pseudo labels. Typically, FixMatch [33] leverages pseudo labels generated from weakly augmented unlabeled images to supervise their strongly augmented versions for robust learning. Moreover, graph-based regularization [43, 44], deep generative models [30, 45, 46, 47] and self-supervised learning [48, 49, 50] are also important branches of semi-supervised learning. Our method builds upon the training frameworks of Mean Teacher [31] and FixMatch [33], illustrating their continued effectiveness.

2.2. Semi-Supervised Semantic Segmentation

The success of SSL can be easily expanded to semantic segmentation with the principles of consistency regularization and pseudo-labeling. PS-MT [19] establishes consistency between two teacher models and a student model and employs a challenging combination of input data, feature and network perturbations to greatly improve the generalization. Instead of introducing an extra network, CCVC [8] relies on a two-branch co-training network to extract features from irrelevant views and enforces consistent predictions through cross-supervision. UniMatch [51] proposes a simple yet effective consistency framework that divides image and feature perturbations

into two independent streams to expand the perturbation space. It further presents a dual-stream strong perturbation to fully explore the pre-defined image-level augmentations. However, due to the density and complexity of semantic segmentation tasks, the generated pseudo labels inevitably contain a large amount of noise, severely limiting the effect of semi-supervised training. A prevalent scheme is to filter out unreliable pseudo labels by setting confidence [28] or entropy thresholds [14]. Besides, some recent studies [21, 22, 52] propose to use an additional error detection network to refine the generated pseudo labels. Nevertheless, most segmentation datasets [29, 32] suffer from a problem of long-tailed class distribution, characterized by extreme pixel-wise class imbalance in training samples. Consequently, deep models trained on such data tend to produce reliable pseudo labels biased to majority classes, further exacerbating the class-bias problem. To address this issue, [53] leverages prior knowledge of the dataset and proposes to align the class distribution of pseudo labels with the true distribution through class-wise thresholding and random sampling. [54] designs a series of adaptive data augmentations, such as adaptive CutMix and Copy-Paste, along with a balanced sampling strategy, to enhance the supervision for under-performing categories. And [55] presents to cluster balanced subclass distributions to train a class-unbiased segmentation model.

Recently, inspired by the effect of contrastive learning, a number of studies have focused on regularizing feature representations in the latent space. ReCo [26] enhances pixel-level contrastive learning by considering semantic relationships between different classes, effectively alleviating the uncertainty among confused classes. U²PL [14], on the other hand, incorporates unre-

liable pixels into the storage queue of negative samples to make full use of unlabeled data. And [56] first proposes a probabilistic representation contrastive learning framework, aiming to mitigate the risk of unreliable pseudo-labels through Gaussian modeling. However, the regularized representations only cover the contextual or batch-level semantics, lacking the category-level ones across the whole dataset. Consequently, the optimization is only implemented on inter-class relationships, overlooking the compactness within each category.

Prototype learning provides an elegant resolution to this issue. Lately, it has been integrated into semantic segmentation due to its concise principle based on nearest neighbors and intuitive interpretability. In particular, [27] first proposes to represent each category with a set of non-learnable class prototypes and make dense predictions via nearest prototype retrieving. PCR [28] applies this scheme to semi-supervised semantic segmentation and achieves remarkable performance, surpassing the existing methods. While our approach further proposes a novel way to generate prototypes with refined class boundaries, and incorporates all steps into a unified training process, leading to significant improvements in performance.

3. Method

3.1. Overview

In semi-supervised semantic segmentation, two sets of data are available for training a segmentation model: a manually labeled dataset $D_L = \{(x_i^l, y_i^l)\}_{i=1}^L$ and an unlabeled dataset $D_U = \{x_i^u\}_{i=1}^U$, where $L \ll U$. Hence, the focus of different methods is how to make full use of massive unlabeled

data. Mean Teacher [31] and pseudo-labeling have emerged as popular solutions to tackle this problem.

These two techniques are also incorporated into the proposed method, which is shown in Fig. 3. The overall framework consists of three main components. In Fig. 3 (a), we present the pre-training stage of the semi-supervised model. In this stage, the Mean Teacher architecture and pseudo-labeling strategy are employed for semi-supervised training, as detailed in Section 3.2. Meanwhile, an extra feature head is introduced to extract pixel-level features from both labeled and unlabeled images. The core idea of our method is demonstrated in Fig. 3 (b) and described in Section 3.3, which includes the process of confidence-based prototype generation (CPG) and adaptive prototype optimization (APO). For CPG, during the sampling stage, high- and low-confidence features are sampled separately based on a confidence threshold and stored in class-wise memory queues. After sampling, K-Means clustering is performed on the two feature queues respectively to generate high- and low-confidence prototypes for each class, consequently bringing the low-confidence prototypes closer to the classification boundaries. Furthermore, APO is applied to make prototype augmentation for classes with dispersed feature distributions. Fig. 3 (c) demonstrates the whole training process with the introduction of prototype-based contrastive learning and specific details are provided in Section 3.4.

3.2. Pre-training

As shown in Fig. 3 (a), the pre-training process of the model is conducted based on the Mean Teacher architecture. Specifically, in addition to the regular network (student network) that is optimized through back-propagation,

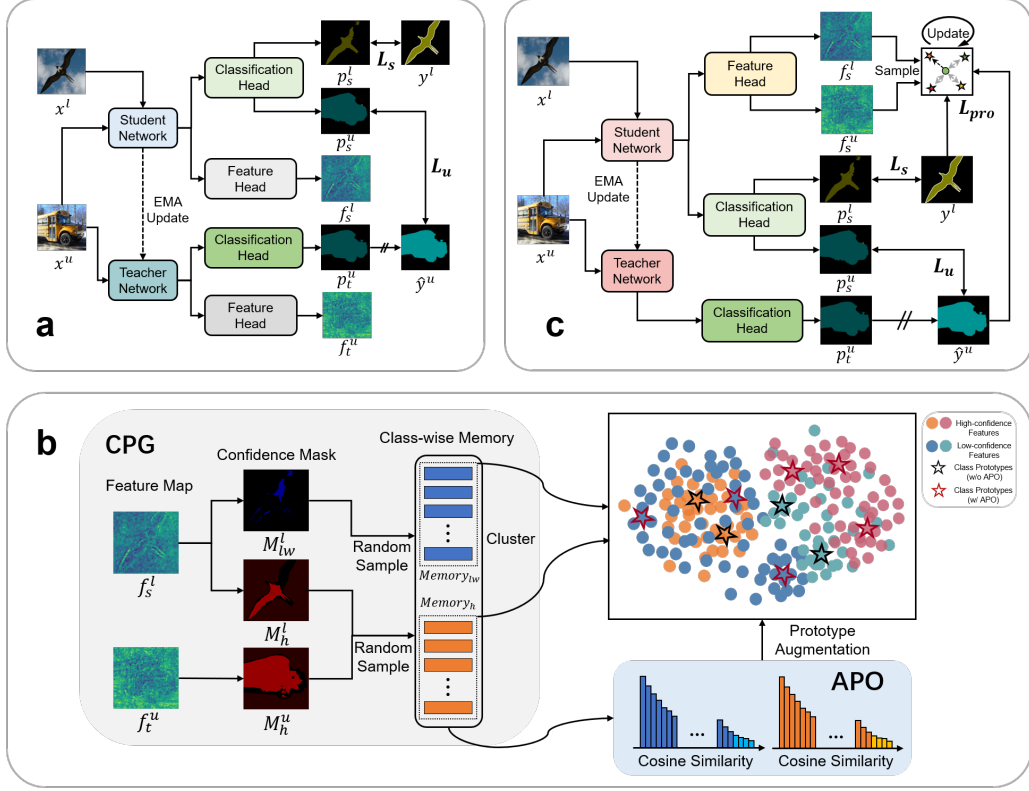


Figure 3: An overview of our training framework. (a) presents the pre-training stage of the Mean Teacher model. (b) shows the proposed boundary-refined prototype generation (BRPG) method with the strategies of confidence-based prototype generation (CPG) (gray region) and adaptive prototype optimization (APO) (blue region). (c) illustrates the overall training process with the generated prototypes.

an extra network with the same architecture, known as the teacher network, is introduced into the semi-supervised framework. The weights of the teacher model are updated as the exponential moving average (EMA) [31] of the student model’s weights, aiming to generate more stable predictions. Each network comprises an encoder E , a decoder with a classification head F , and a feature head G .

Given a batch of B_l labeled samples $\{(x_i^l, y_i^l)\}_{i=1}^{B_l}$, the supervised loss function can be defined as:

$$L_s = \frac{1}{B_l} \frac{1}{HW} \sum_{i=1}^{B_l} \sum_{j=1}^{HW} l_{ce}(p_{s,ij}^l, y_{ij}^l), \quad (1)$$

where $p_{s,ij}^l = \text{Softmax}(F \circ E(x_{ij}^l))$ denotes the predicted probabilities by the student model for the j -th pixel of the i -th labeled image. Here, $F \circ E$ is the joint mapping of the encoder E and the classification head F . The ground-truth label for this pixel is denoted as y_{ij}^l , and the cross-entropy loss is computed using the function $l_{ce}(\cdot, \cdot)$. H and W represent the height and width of the image, respectively.

For the unlabeled images $\{x_i^u\}_{i=1}^{B_u}$, the pseudo-labeling strategy is adopted to extend the supervision of the student model training. In particular, the predictions of the teacher model are used to generate pseudo labels as follows:

$$\hat{y}_{ij}^u = \underset{c}{\operatorname{argmax}}(p_{t,ij}^u), \quad (2)$$

where $p_{t,ij}^u = \text{Softmax}(\hat{F} \circ \hat{E}(x_{ij}^u))$ represents the softmax probabilities generated by the teacher network.

To ensure the high quality of pseudo labels, it is common to introduce a confidence threshold η or an entropy threshold β to filter out potential noise. For unlabeled images, the pseudo label mask is defined as follows:

$$M_{ij}^u = \mathbb{1}(\max(p_{t,ij}^u) \geq \eta) \quad (3)$$

or

$$M_{ij}^u = \mathbb{1}(\mathcal{H}(p_{t,ij}^u) < \beta), \quad (4)$$

where $\mathcal{H}(\cdot)$ represents the pixel-level entropy function. Pixels that satisfy the confidence or entropy condition are assigned a value of 1, while the remaining ones are set as 0. In this way, the unsupervised loss function guided by pseudo labels can be formulated as:

$$L_u = \frac{1}{M} \sum_{i=1}^{B_u} \sum_{j=1}^{HW} l_{ce}(p_{s,ij}^u, \hat{y}_{ij}^u) \cdot M_{ij}^u, \quad (5)$$

where $M = \sum_{i=1}^{B_u} \sum_{j=1}^{HW} M_{ij}^u$ indicates the total number of pixels involved in the loss calculation, and $p_{s,ij}^u = \text{Softmax}(F \circ E(x_{ij}^u))$ denotes the predictions of the student model for unlabeled data.

Thus, in the pre-training stage, the total loss function can be formulated as follows:

$$L = L_s + \lambda_u L_u, \quad (6)$$

where λ_u is the weight of unsupervised loss.

Note that during pre-training, the segmentation model also extracts features from both labeled and unlabeled images to facilitate subsequent sampling and prototype generation. Specifically, the features extracted by the student model from the i -th labeled image can be represented as $f_{s,i}^l = G \circ E(x_i^l)$. Meanwhile, to ensure robustness, the features for unlabeled images are consistently obtained from the teacher model, and the resulting feature map is denoted as $f_{t,i}^u = \hat{G} \circ \hat{E}(x_i^u)$.

3.3. Boundary-Refined Prototype Generation (BRPG)

In this section, a novel online Boundary-Refined Prototype Generation (BRPG) method is proposed to clarify the initial class boundaries of the model. As shown in Fig. 3 (b), BRPG consists of two main components,

namely CPG and APO, which will be discussed in Section 3.3.1 and Section 3.3.2, respectively.

3.3.1. Confidence-Based Prototype Generation (CPG)

Prototype-based learning [57, 58] is a classical approach in machine learning, which has evolved from the nearest neighbors algorithm [59] and the prototype theory [60, 61] in cognitive science. It has achieved notable success in semantic segmentation tasks [62, 63, 64]. The core is to abstract each class as a set of non-learnable prototypes and perform classification by comparing samples to these prototypes. Thus, the initialization strategy for prototypes plays an important role in the classification task.

Experimental results in [30] have demonstrated the significant improvement in model classification by refining the class boundaries. Inspired by their findings, we aim to initialize a specific number of prototypes in sparse regions of feature distributions for each class. This method enables the prototypes to capture more challenging samples and refine the class boundaries in prototype-based learning. Fig. 2 has illustrated that low-confidence features tend to depart more from the category center, while Fig. 1 has directly shown that low-confidence prototypes locate closer to the class boundaries, which is consistent with our research goal. Consequently, a confidence-based prototype generation (CPG) strategy is proposed, which is depicted in the gray region of Fig. 3 (b).

Specifically, during the sampling stage, for the features f_s^l and f_t^u generated in pre-training, a confidence threshold is introduced to facilitate sampling high- and low-confidence features separately. Besides, in order to maintain a stable number of samples for each class, two category-wise memory

banks (FIFO queues), i.e., $Memory_h$ and $Memory_{lw}$, are utilized to store these features. Formally, the whole process for high-confidence features can be described as follows:

$$Memory_h^{(t)} = Q \left(Memory_h^{(t-1)}, S \left(\{f_{s,h,i}^l\}_{i=1}^{B_l}, \{f_{t,h,i}^u\}_{i=1}^{B_u} \right) \right), \quad (7)$$

where $f_{s,h,i}^l$ denotes the high-confidence features extracted from the i -th labeled image by the student model and $f_{t,h,i}^u$ represents those extracted from the i -th unlabeled image by the teacher model. In the case of labeled images, pixels are classified as “high confidence” based on two conditions: (1) the predicted label belongs to the same class as the ground truth, and (2) the softmax probability for the predicted class (i.e., confidence probability) is not less than $\eta_s = 0.8$. For unlabeled images, high-confidence features are solely required to have a confidence probability of not less than 0.8, since the ground-truth labels are unavailable.

S denotes the random sampling of high-confidence features with a maximum quantity limit of $(B_l + B_u) * sample_num$, where $sample_num$ is set to 5000. Q is the first-in-first-out (FIFO) operation of the storage queues for each class, facilitating the dynamic update of features.

For low-confidence features, sampling is only performed on labeled images to avoid noise:

$$Memory_{lw}^{(t)} = Q \left(Memory_{lw}^{(t-1)}, \hat{S} \left(\{f_{s,lw,i}^l\}_{i=1}^{B_l} \right) \right), \quad (8)$$

where $f_{s,lw,i}^l$ represents the low-confidence features of labeled images, which satisfy the condition of correct predictions but have confidence probabilities lower than $\eta_s = 0.8$. The maximum sampling limit for \hat{S} is set to $B_l *$

sample_num. Besides, both memory banks have a storage capacity of $V = 30000$ for each class.

After the sampling stage, the K-Means clustering algorithm is applied to both of the memory banks to generate high- and low-confidence cluster centers for each category, which serve as class prototypes. This can be formulated as follows:

$$R_c = \{ \text{Cluster} (Memory_{h,c}, N_{h,c}), \text{Cluster} (Memory_{lw,c}, N_{lw,c}) \} = \{r_{c,k}\}_{k=1}^{N_c}, \quad (9)$$

where $N_{h,c}$ and $N_{lw,c}$ denote the number of high- and low-confidence cluster centers for class c , respectively, so the total number is $N_c = N_{h,c} + N_{lw,c}$.

3.3.2. Adaptive Prototype Optimization (APO)

Considering the variation in feature diversity among different categories, assigning an equal number of prototypes to each class may not be the optimal solution. To address this, a simple yet effective technique called Adaptive Prototype Optimization (APO) is proposed, as shown in the blue region of Fig. 3 (b). APO aims to increase the number of cluster centers for classes with more scattered feature distributions, thereby enhancing the refinement of classification boundaries in prototype-based learning. To measure the dispersion of features, two indicators are taken into account: cosine similarity and l_2 distance.

Specifically, for the cosine similarity indicator, the average cosine similarity between the features and the class center is calculated for each category. The dispersion score for category c is computed as follows:

$$D_{sim,\alpha,c} = \frac{1}{V_{\alpha,c}} \sum_{f \in Memory_{\alpha,c}} \langle f, \bar{f} \rangle, \quad (10)$$

where $\langle \cdot, \cdot \rangle$ denotes the similarity metric function and $\alpha \in \{h, lw\}$ indicates that the dispersion scores of high- and low-confidence features are calculated separately. $V_{\alpha,c}$ is the actual number of stored samples, while $\bar{f} = \frac{1}{V_{\alpha,c}} \sum_{f \in Memory_{\alpha,c}} f$ represents the class center. A lower dispersion score indicates a more scattered feature distribution.

The dispersion scores for all categories can be represented as $D_{sim,\alpha} = \{D_{sim,\alpha,c}\}_{c=1}^C$, and an additional cluster center will be added to the categories whose scores are on the bottom α_t . Thus, the prototype number $N_{\alpha,c}$ ($\alpha \in \{h, lw\}$) in Eq. (9) can be defined as:

$$N_{\alpha,c} = n_{0\alpha} + \mathbb{1}(D_{sim,\alpha,c} < \gamma_t), \quad (11)$$

where γ_t denotes the quantile threshold corresponding to α_t , i.e., $\gamma_t = np.percentile(D_{sim,\alpha}, 100 * \alpha_t)$, where α_t is set to 5%. Besides, $n_{0\alpha}$ is the pre-defined number of prototypes, which is set to 2 for all the experiments.

Similarly, for the $l2$ distance indicator, the dispersion score can be formulated as:

$$D_{l2,\alpha,c} = \frac{1}{V_{\alpha,c}} \sum_{f \in Memory_{\alpha,c}} \|f - \bar{f}\|_2, \quad (12)$$

where $\|\cdot\|_2$ represents the $l2$ norm. Unlike the case of cosine similarity indicator, a higher dispersion score based on $l2$ distance indicates a more scattered feature distribution. Hence, for the dispersion scores $D_{l2,\alpha} = \{D_{l2,\alpha,c}\}_{c=1}^C$, only the top α_t categories are eligible to have an additional prototype:

$$N_{\alpha,c} = n_{0\alpha} + \mathbb{1}(D_{l2,\alpha,c} > \gamma_t), \quad (13)$$

where the threshold $\gamma_t = np.percentile(D_{l2,\alpha}, 100 * (1 - \alpha_t))$.

Note that the cosine similarity indicator exhibits better performance in our method, and therefore, it is adopted by default (refer to Section 4.3 for the comparison).

3.4. Training with Prototype-Based Contrastive Learning

With the class prototypes generated by BRPG, the semi-supervised model can be regularized by incorporating prototype-based contrastive learning, as illustrated in Fig. 3 (c).

It is worth noting that the prototype-based classifier (feature head) and the parameterized classifier (classification head) have distinct decision mechanisms for semantic segmentation. Specifically, the parameterized classifier allocates learnable parameters to different dimensions of the extracted feature representations, enabling it to focus more on discriminative dimensions while suppressing irrelevant ones. This may lead to overfitting to the specific feature dimensions, thereby hindering the generalization of the model. In contrast, the prototype-based classifier regards all dimensions equally and solely relies on the similarities between features and prototypes when making predictions. Therefore, it is beneficial to introduce prototype-based learning as an auxiliary branch, which promotes the generation of more robust features and enhances the model’s generalization performance. Following [28], the prototype-based contrastive learning algorithm is designed as follows:

Due to the dense predictions in semantic segmentation, it is computationally expensive to compare the features of each pixel with prototypes. To tackle this issue, grid sampling is adopted for labeled images to compute the cosine similarities between the sampled features and prototypes. Particularly, the similarity between the sampled feature i extracted by the feature head

and category c is defined as the maximum similarity among all prototypes of category c , which can be formulated as:

$$s_{i,c} = \max \{ \langle i, r_{c,k} \rangle \}_{k=1}^{N_c}. \quad (14)$$

In this case, the probability of assigning sample i to class c can be estimated in the student model’s feature head via:

$$p_{i,c}^{pro} = \frac{\exp(s_{i,c}/\tau)}{\sum_{t=1}^C \exp(s_{i,t}/\tau)}, \quad (15)$$

where C represents the number of classes, and τ is the temperature coefficient, which is set to 0.1, same as [28].

Therefore, the loss function on labeled data is formulated as follows:

$$\begin{aligned} L_{pro}^l &= - \frac{1}{B_l \times M_l} \sum_{i=1}^{B_l} \sum_{j=1}^{M_l} \log p_{ij, y_{ij}^l}^{pro} \\ &= - \frac{1}{B_l \times M_l} \sum_{i=1}^{B_l} \sum_{j=1}^{M_l} \log \frac{\exp(s_{ij, y_{ij}^l} / \tau)}{\sum_{t=1}^C \exp(s_{ij, t} / \tau)}, \end{aligned} \quad (16)$$

where M_l denotes the number of sampled features per labeled image. Note that the granularity of grid sampling is set to 32, resulting in a total of 32×32 samples in each image.

For unlabeled data, to promote the consistency between the two heads, we utilize the pseudo labels generated by the teacher model’s classification head to guide the prototype-based learning:

$$\begin{aligned} L_{pro}^u &= - \frac{1}{B_u \times M_u} \sum_{i=1}^{B_u} \sum_{j=1}^{M_u} \log p_{ij, \hat{y}_{ij}^u}^{pro} \\ &= - \frac{1}{B_u \times M_u} \sum_{i=1}^{B_u} \sum_{j=1}^{M_u} \log \frac{\exp(s_{ij, \hat{y}_{ij}^u} / \tau)}{\sum_{t=1}^C \exp(s_{ij, t} / \tau)}, \end{aligned} \quad (17)$$

$$\text{s.t. } \max(p_{t,ij}^u) \geq \eta_t,$$

where M_u denotes the number of randomly sampled features per unlabeled image, with a fixed value of 1000 to match the sampling size of labeled data. Moreover, to mitigate overfitting to the noise in pseudo labels, the sampling is restricted to pixels whose confidence probabilities are not less than the threshold η_t .

However, during the training procedure, the confidence of pseudo labels tends to increase gradually. Based on this intuition, a linear strategy is leveraged to incrementally adjust the threshold η_t at each iteration:

$$\eta_t = \eta_0 + (\eta_e - \eta_0) \frac{\text{curr_iter}}{\text{total_iter}}, \quad (18)$$

where η_0 and η_e denote the initial and final thresholds, which are set to 0.8 and 0.95. curr_iter and total_iter represent the number of completed iterations and the total number of iterations, respectively, after the sampling stage.

Therefore, the overall loss for prototype-based contrastive learning is defined as:

$$L_{pro} = L_{pro}^l + L_{pro}^u. \quad (19)$$

The total loss function with L_{pro} can be formulated as:

$$L = L_s + \lambda_u L_u + \lambda_{pro} L_{pro}, \quad (20)$$

where the weight parameter λ_{pro} is set to 1.

Moreover, in our method, the prototypes are dynamically updated with the $M_l + M_u$ features sampled from both labeled and unlabeled images, ensuring their compatibility with the evolving model. For labeled data, each

sampled feature is used to update the most similar prototype within the same category. In the case of unlabeled features, the categories of their pseudo labels are leveraged as references due to the unavailability of ground truths. The update of each prototype can be formally defined as:

$$r_{c,k}^{(t)} = \alpha \cdot r_{c,k}^{(t-1)} + (1 - \alpha) \cdot \bar{f}_{c,k}, \quad (21)$$

where $\bar{f}_{c,k}$ is the mean value of all the features assigned to this prototype, and the hyper-parameter α , which controls the update speed, is set to 0.99.

Finally, the whole pipeline of our method is shown in Algorithm 1, where the process of BRPG is described from line 8 to line 17.

Algorithm 1 An overview of our approach

Input: D_L : labeled dataset, D_U : unlabeled dataset

Output: the parameters of the teacher network

Initialization: T : total number of epochs, $[T_{S1}, T_{S2}]$: the epoch range for sampling, n_{iter} : the number of iterations per epoch, B_l : batch size of labeled data, B_u : batch size of unlabeled data, λ_u : weight of unsupervised loss, λ_{pro} : weight of prototype-based loss

Process:

- 1: **for** $e \leftarrow 0$ **to** $T - 1$ **do**
- 2: **for** $i \leftarrow 0$ **to** $n_{iter} - 1$ **do**
- 3: Sample a batch of labeled data $\{(x_i^l, y_i^l)\}_{i=1}^{B_l}$ and unlabeled data $\{x_i^u\}_{i=1}^{B_u}$ from $D_L \cup D_U$
- 4: Calculate the supervised loss L_S based on Eq. (1)
- 5: Calculate the unsupervised loss L_u based on Eq. (5)
- 6: Calculate the overall loss $L \leftarrow L_S + \lambda_u L_u$

- 7: Extract features $\{f_{s,i}^l\}_{i=1}^{B_l}$ and $\{f_{t,i}^u\}_{i=1}^{B_u}$ from both labeled and unlabeled images
- 8: **if** $e \geq T_{S1}$ **and** $e < T_{S2}$ **then**
- 9: Obtain high-confidence features $\{f_{s,h,i}^l\}_{i=1}^{B_l}$ and low-confidence features $\{f_{s,lw,i}^l\}_{i=1}^{B_l}$ of labeled data via the confidence mask
- 10: Obtain high-confidence features $\{f_{t,h,i}^u\}_{i=1}^{B_u}$ of unlabeled data via the confidence mask
- 11: Sample and store the high-confidence features in $Memory_h$ based on Eq. (7)
- 12: Sample and store the low-confidence features in $Memory_{lw}$ based on Eq. (8)
- 13: **else**
- 14: **if** $e = T_{S2}$ **and** $i = 0$ **then**
- 15: Calculate the prototype number $N_{\alpha,c}$ for each category based on Eq. (10) and Eq. (11)
- 16: Perform K-Means clustering on memory banks to generate prototypes R_c based on Eq. (9)
- 17: **end if**
- 18: Extract features of labeled images from the feature head of the student network and perform grid sampling on them
- 19: Calculate the loss function of prototype-based contrastive learning L_{pro}^l on labeled data based on Eq. (16)
- 20: Extract features of unlabeled images from the feature head of the student network and perform random sampling via the confidence threshold η_t

21: Calculate the loss function of prototype-based contrastive learning L_{pro}^u on unlabeled data based on Eq. (17)

22: Calculate the total prototype-based loss $L_{\text{pro}} \leftarrow L_{\text{pro}}^l + L_{\text{pro}}^u$

23: Update the prototypes R_c for each category based on Eq. (21)

24: Update the overall loss $L \leftarrow L + \lambda_{\text{pro}} L_{\text{pro}}$

25: **end if**

26: Update the student network through back-propagation

27: Update the teacher network via EMA of the student network’s parameters

28: **end for**

29: **end for**

4. Experiments

4.1. Setup

Datasets. PASCAL VOC 2012 [29] is a benchmark dataset used for visual object segmentation, which contains 20 foreground categories along with a background category. The training set and the validation set consist of 1,464 and 1,449 finely annotated images, respectively. Later, the extra 9,118 coarsely annotated training images from the SBD dataset [65] are introduced to extend the original dataset, resulting in a total of 10,582 training images. Following the previous studies [14, 28, 51] in semi-supervised semantic segmentation, our experiments are conducted on two settings, i.e., the classic setting and the blended setting. Specifically, the former selects labeled images only from the finely annotated set with 1,464 samples, while the latter selects from the extended set with all 10,582 labeled images.

Cityscapes [32] is a standard dataset designed for urban scene segmentation. It comprises a total of 2,975 training images and 500 validation images, covering 19 different semantic categories. All images in the dataset have a consistent resolution of 2048×1024 pixels.

For each dataset, the proposed approach is evaluated under 1/16, 1/8, 1/4, and 1/2 partition protocols, and compared with the state-of-the-art (SOTA) methods under the same data splits from U²PL [14] for a fair comparison.

Network Architecture. Following the previous works [14, 28], both the student and teacher networks adopt ResNet-101 [66] pretrained on ImageNet [67] as the backbone and Deeplabv3+ [68] as the decoder. Similar to the inherent classification head, an extra feature head is appended following the ASPP module [4]. Both heads are composed of two Conv-BN-ReLU-Dropout blocks. However, the feature head differs in mapping the shared features to a 256-dimensional representation space instead of the label space.

Evaluation Protocols. All evaluations are conducted with the classification head of the teacher network. For PASCAL VOC 2012, single-scale evaluation is performed on the center-cropped images, while for Cityscapes, sliding window evaluation is employed to preserve the original image resolution. Then the mean of Intersection of Union (mIoU) is adopted as the metric to assess the segmentation performance of our model. The reported results are measured on the validation sets of both datasets.

Implementation Details. We utilize the stochastic gradient descent (SGD) optimizer for training on both datasets. For PASCAL VOC 2012, the initial learning rates of the backbone and decoder are 0.001 and 0.01,

respectively. The momentum is set to 0.9, weight decay to 0.0001, and the batch size is $B_l = B_u = 16$. The model is trained for 80 epochs. For training on Cityscapes, the entire model has an initial learning rate of 0.005, with a momentum of 0.9 and weight decay of 0.0005. The batch size is set to $B_l = B_u = 8$, and the model is trained for 200 epochs. Throughout the training process, a polynomial policy is used to dynamically decay the learning rate: $lr = lr_{init} \cdot \left(1 - \frac{i_iter}{total_i_iter}\right)^{0.9}$.

The pre-training setting of our model follows U²PL [14]. To enhance the robustness, data augmentations are applied to both labeled and unlabeled data, including random resize, random horizontal flip and random crop. Concretely, the input images are first randomly resized between 0.5 and 2.0, then horizontally flipped with a 0.5 probability, and finally cropped to the designated size. For PASCAL VOC 2012, the crop size is set to 513×513 , while for Cityscapes, it is set to 769×769 . Furthermore, following [51], strong augmentations, including Color Jitter and CutMix are applied for the consistency training of unlabeled data. In particular, to ensure high-quality features, the feature sampling is conducted after a few epochs of network warm-up. For the PASCAL dataset, the sampling range is set as $T_{S1} = 1$ and $T_{S2} = 2$. For Cityscapes, T_{S1} and T_{S2} are set to 3 and 6, respectively, to account for the fewer iterations within an epoch.

Note that all of our experiments are conducted on four NVIDIA Tesla V100 GPUs. However, due to the limitation of hardware memory, the experimental results can only be reported using mixed precision training [69].

Table 1: Comparison with the SOTA methods on **PASCAL VOC 2012** *val* set under different partition protocols. Methods are trained on the *classic* setting, i.e., labeled images are selected from the high-quality training set with 1,464 samples. The fractions represent the proportion of labeled data used for training, followed by the corresponding number of images.

Method	1/16(92)	1/8(183)	1/4(366)	1/2(732)	Full(1464)
SupOnly	45.77	54.92	65.88	71.69	72.50
MT [31] <small>[NeurIPS'17]</small>	51.72	58.93	63.86	69.51	70.96
CutMix-Seg [13] <small>[BMVC'20]</small>	52.16	63.47	69.46	73.73	76.54
PseudoSeg [20] <small>[ICLR'21]</small>	57.60	65.50	69.14	72.41	73.23
PC ² Seg [25] <small>[ICCV'21]</small>	57.00	66.28	69.78	73.05	74.15
CPS [9] <small>[CVPR'21]</small>	64.07	67.42	71.71	75.88	-
ReCo [26] <small>[ICLR'22]</small>	64.78	72.02	73.14	74.69	-
ST++ [23] <small>[CVPR'22]</small>	65.20	71.00	74.60	77.30	79.10
U ² PL [14] <small>[CVPR'22]</small>	67.98	69.15	73.66	76.16	79.49
PS-MT [19] <small>[CVPR'22]</small>	65.80	69.58	76.57	78.42	80.01
GTA-Seg [70] <small>[NeurIPS'22]</small>	70.02	73.16	75.57	78.37	80.47
PCR [28] <small>[NeurIPS'22]</small>	70.06	74.71	77.16	78.49	80.65
PRCL [56] <small>[AAAI'23]</small>	69.91	74.42	76.69	-	-
CCVC [8] <small>[CVPR'23]</small>	70.20	74.40	77.40	79.10	80.50
FPL [71] <small>[CVPR'23]</small>	69.30	71.72	75.73	78.95	-
Forec [72] <small>[arXiv'23]</small>	71.00	74.70	77.50	78.70	81.10
BRPG <small>[Ours]</small>	73.62	76.55	78.00	79.78	81.91

Table 2: Comparison with the SOTA methods on **PASCAL VOC 2012** *val* set under different partition protocols. Methods are trained on the *blended* setting, i.e., labeled images are selected from the extended training set with 10,582 samples in total.

Method	1/16(662)	1/8(1323)	1/4(2646)	1/2(5291)
SupOnly	67.87	71.55	75.80	77.13
MT [31] <small>[NeurIPS'17]</small>	70.51	71.53	73.02	76.58
CutMix-Seg [13] <small>[BMVC'20]</small>	71.66	75.51	77.33	78.21
CCT [18] <small>[CVPR'20]</small>	71.86	73.68	76.51	77.40
GCT [52] <small>[ECCV'20]</small>	70.90	73.29	76.66	77.98
CPS [9] <small>[CVPR'21]</small>	74.48	76.44	77.68	78.64
AEL [54] <small>[NeurIPS'21]</small>	77.20	77.57	78.06	80.29
U ² PL [14] <small>[CVPR'22]</small>	77.21	79.01	79.30	80.50
GTA-Seg [70] <small>[NeurIPS'22]</small>	77.82	80.47	80.57	81.01
PCR [28] <small>[NeurIPS'22]</small>	78.60	80.71	80.78	80.91
CCVC [8] <small>[CVPR'23]</small>	76.80	79.40	79.60	-
Forec [72] <small>[arXiv'23]</small>	78.84	80.52	80.92	80.99
BRPG <small>[Ours]</small>	79.40	81.61	81.83	80.78

4.2. Comparison with State-of-the-Art Methods

In this section, the proposed method is compared with the SOTA semi-supervised semantic segmentation methods. For a fair comparison, all the methods are equipped with the DeepLabV3+ network with ResNet-101 as the backbone. The experimental results on the classic and blended settings of PASCAL VOC 2012 and Cityscapes are presented in Table 1, Table 2, and Table 3, respectively. Note that all the reported results are the average of

Table 3: Comparison with the SOTA methods on **Cityscapes** *val* set under different partition protocols. All labeled images are selected from the Cityscapes *train* set with 2,975 samples in total.

Method	1/16 (186)	1/8 (372)	1/4 (744)	1/2 (1488)
SupOnly	65.74	72.53	74.43	77.83
MT [31] <small>[NeurIPS'17]</small>	69.03	72.06	74.20	78.15
CutMix-Seg [13] <small>[BMVC'20]</small>	67.06	71.83	76.36	78.25
CCT [18] <small>[CVPR'20]</small>	69.32	74.12	75.99	78.10
GCT [52] <small>[ECCV'20]</small>	66.75	72.66	76.11	78.34
CPS [9] <small>[CVPR'21]</small>	69.78	74.31	74.58	76.81
AEL [54] <small>[NeurIPS'21]</small>	74.45	75.55	77.48	79.01
U ² PL [14] <small>[CVPR'22]</small>	70.30	74.37	76.47	79.05
PS-MT [19] <small>[CVPR'22]</small>	-	76.89	77.60	79.09
GTA-Seg [70] <small>[NeurIPS'22]</small>	69.38	72.02	76.08	-
PCR [28] <small>[NeurIPS'22]</small>	73.41	76.31	78.40	79.11
CISC-R [73] <small>[TPAMI'23]</small>	-	75.89	77.65	-
UniMatch [51] <small>[CVPR'23]</small>	76.60	77.90	79.20	79.50
RRN [74] <small>[ICME'23]</small>	75.42	77.34	78.38	79.09
Forec [72] <small>[arXiv'23]</small>	72.42	75.76	77.65	79.18
BRPG <small>[Ours]</small>	76.37	78.56	79.46	80.26

three experiments.

Results on PASCAL VOC 2012 Dataset. Table 1 presents the comparison results on the classic setting of PASCAL VOC 2012. Our method exhibits substantial improvements over the supervised baseline by +27.85%,

+21.63%, +12.12%, +8.09%, and +9.41% under the five label partitions, respectively. Moreover, compared with the previous best prototype-based method PCR [28], our approach still yields superior performance, with gains of +3.56%, +1.84%, +0.84%, +1.29%, and +1.26% under each partition, respectively. It confirms that the proposed end-to-end method can completely achieve and even surpass the existing method with offline prototype generation. Besides, our method outperforms the previous best results across all partitions, particularly on low-data regimes, e.g., +2.62% and +1.84% under 1/16 and 1/8 partitions, respectively.

Table 2 reports the comparison results on the blended setting. It is obvious that our proposed approach consistently outperforms the supervised baseline by a large margin. For instance, our method surpasses the SupOnly baseline by over 10% mIoU under both 1/16 and 1/8 partitions. Compared with the prototype-based method PCR [28], our approach performs better under 1/16, 1/8, and 1/4 partitions, with the improvements of +0.8%, +0.9%, and +1.05%, respectively, and achieves a comparable result under 1/2 label partition. Furthermore, our proposed method is superior to previous best results under most partitions.

However, it is worth noting that the performance of our method appears to drop under 1/2 partition protocol, which is also slightly inferior to the previous best. It may be attributed to the reduced number of unlabeled images, leading to fewer iterations per epoch (as the number of epochs is calculated based on the iterations of unlabeled images). Furthermore, we have observed that the network performance does not reach saturation throughout the whole training. Hence, a better result may be obtained with a longer

training process.

Results on Cityscapes Dataset. Table 3 illustrates the comparison results on Cityscapes. Our approach achieves remarkable performance gains over the SupOnly approach by +10.63%, +6.03%, +5.03%, and +2.43% under the 1/16, 1/8, 1/4, and 1/2 partition protocols, respectively. In addition, our method outperforms PCR [28] under all partitions by +2.96%, +2.25%, +1.06%, and +1.15%, respectively. Notably, our proposed method excels over the SOTA algorithm UniMatch [51] by +0.66%, +0.26%, and +0.76% under 1/8, 1/4, and 1/2 partitions, respectively, with only a slight disadvantage of 0.23% under 1/16 partition. These results indicate the overall superiority of the proposed method.

Results on PASCAL VOC 2012 and Cityscapes demonstrate the advancement of our approach. Particularly, the remarkable improvements over PCR [28] indicate the effectiveness of the novel BRPG method in prototype-based learning for semi-supervised training.

4.3. Ablation Study

To investigate the effectiveness of the proposed modules and the impact of various configurations, ablation studies are conducted on 1/4 (366) split of the classic setting and 1/8 (1323) split of the blended setting in PASCAL VOC 2012.

Effectiveness of Components. To manifest the contribution of each component, a series of ablation experiments are conducted as shown in Table 4. Among them, two baseline models, trained with SupOnly manner (Experiment I) and pseudo-labeling (Experiment II), are employed for comparison. In Experiment III, the proposed end-to-end prototype-based contrastive

learning is introduced to the semi-supervised model with random sampling and prototype generation, leading to performance improvements of +1.62% and +1.11% under 366 and 1323 partitions, respectively. Experiment IV demonstrates the effect of incorporating the confidence-based prototype generation (CPG) strategy, which further improves the performance by +0.62% and +0.21%. This can be attributed to the scheme of separate sampling and clustering based on high and low confidences. Finally, in Experiment V, the adaptive prototype optimization (APO) method is leveraged to make prototype augmentation for categories with dispersed feature distributions, resulting in gains of +0.61% and +0.41% on the two splits, respectively. It is noteworthy that the proposed novel approach BRPG (CPG+APO) exhibits significant improvements over Model III with a total gain of +1.23% and +0.62% under the two partitions, respectively. This observation indicates the importance of refining initial class boundaries in prototype-based learning.

Value of the confidence threshold η_s . Based on the confidence threshold η_s , the separate sampling of high- and low-confidence features constitutes a fundamental element of our method. In order to explore the impact of η_s on model performance, ablation studies are conducted with its different values as shown in Table 5. It can be observed that within the range of [0.7, 0.95], $\eta_s = 0.8$ yields the best results, while other values are also acceptable.

Moreover, considering the performance variations across different classes, the investigation also explores the effect of setting class-specific confidence thresholds. Specifically, an initial threshold of 0.8 is assigned to each class, with upper and lower bounds of 0.9 and 0.7, respectively. Subsequently,

Table 4: Ablation study on different components of the proposed approach. L_{sup} : Supervised training with labeled data. L_{unsup} : Unsupervised training with pseudo labels. L_{pro} : Plain prototype-based contrastive learning with random sampling and direct K-Means clustering. CPG: Confidence-based prototype generation. APO: Adaptive prototype optimization.

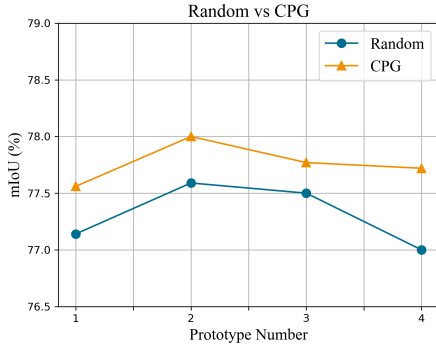
	L_{sup}	L_{unsup}	L_{pro}	CPG	APO	366	1323
I	✓					65.88	71.55
II	✓	✓				75.15	79.88
III	✓	✓	✓			76.77	80.99
IV	✓	✓	✓	✓		77.39	81.20
V	✓	✓	✓	✓	✓	78.00	81.61

Table 5: Ablation study on the value of confidence threshold η_s during the sampling stage. All the experiments are conducted on (1/4) 366 split of PASCAL VOC 2012.

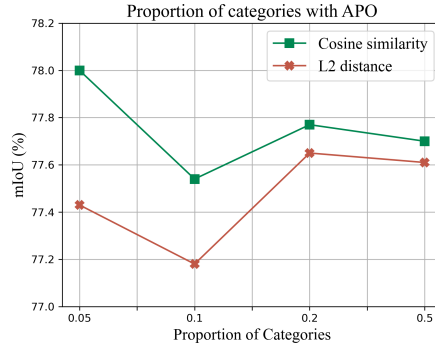
η_s	0.7	0.75	0.8	0.85	0.9	0.95	EMA _{0.7-0.9}
mIoU	77.59	77.69	78.00	77.50	77.86	77.51	78.14

the thresholds are updated during the sampling stage using the EMA [31] strategy with a decay rate of 0.999, based on the mean confidence predicted for each category. As presented in Table 5, this approach exhibits a marginal improvement compared to the model with $\eta_s = 0.8$. Therefore, future work could focus on identifying optimal solutions for class-specific confidence thresholding.

Strategies for prototype generation. Fig. 4 (a) presents the impacts of prototype generation strategies and the number of prototypes. It demonstrates that the proposed confidence-based prototype generation (CPG) method



(a) Random vs CPG



(b) Proportion of categories with APO

Figure 4: Ablation studies on CPG and APO. (a) shows the comparison between the two prototype generation methods under different number of prototypes. Random: Random sampling and direct K-Means clustering. CPG: Confidence-based prototype generation. Note that the “Prototype Number” for the “Random” strategy indicates the number of prototypes per category, while for “CPG”, it denotes the number of high- and low-confidence prototypes, respectively, for each category. Despite this difference, it is evident that CPG consistently outperforms the baseline. (b) presents the performance of APO under different class proportions, considering two indicators: cosine similarity and l_2 distance. All the results presented are obtained using (1/4) 366 split of PASCAL VOC 2012.

consistently outperforms the baseline method, which involves random feature sampling and direct K-Means clustering. Besides, optimal performance can be obtained when setting the number of high- and low-confidence prototypes to 2 for each category in CPG, respectively, which is also the default value in our experiments.

Proportion of categories with APO. APO aims to increase the number of cluster centers for categories with scattered feature distributions. Hence, it is crucial to select a reliable indicator that measures the disper-

sion of features. As aforementioned, two indicators are taken into account, i.e., cosine similarity and l_2 distance. Based on the two indicators, the ablation studies on the class proportions for implementing APO are illustrated in Fig 4 (b). It can be seen that the cosine similarity indicator achieves superior performance in our method, and the optimal result is reached when the class proportion is set to 5%.

Table 6: Ablation study on different configurations for the sampling stage. Baseline (Ours): Feature head is not pre-trained. Experiment I: Pretrain the feature head with labeled data before the sampling stage. Experiment II: Extract features from the classification head. Experiment III: Extract features from the ASPP module, discarding the feature head.

Split	Baseline (Ours)	Experiment I	Experiment II	Experiment III
366	78.00	77.24	77.60	77.17
1323	81.61	81.81	81.23	80.81

Configurations for the sampling stage. Note that the feature head of the proposed method is not pretrained before the sampling stage, so the extracted features solely rely on the shared features and the initial parameters of this sub-net. To examine the effect of the feature head and sampled features on the final results, we conduct experiments under the following settings: (1) Pretrain the feature head with labeled data before the sampling stage. (2) Extract features from the classification head. (3) Extract 512-dimensional features from the output of ASPP module, discarding the feature head. Table 6 presents the experimental results comparing these configurations with our baseline method. It can be observed that network pretraining (Experiment I) or the use of discriminative features (Experiment II) does not lead to significant performance improvements and may even

cause slight degradation. Additionally, extracting features from ASPP for prototype-based training (Experiment III) results in inferior performance, which indicates the necessity of introducing the feature head. Consequently, the baseline setting is adopted as the default in our experiments.

Table 7: Scalability validation using the FixMatch framework on the *classic* setting of **PASCAL VOC 2012**. † means we use the results reported in [51].

Method	92	183	366	732	1464
FixMatch†	63.90	73.00	75.50	77.80	79.20
FixMatch+BRPG	67.45	74.71	76.47	78.57	79.70
Gain(Δ)	\uparrow 3.55	\uparrow 1.71	\uparrow 0.97	\uparrow 0.77	\uparrow 0.50

4.4. Scalability Validation

In this section, the proposed method is applied to another prevalent semi-supervised self-training framework, FixMatch [33], to validate its scalability. Similar to the utilization of Mean Teacher [31], an additional feature head is incorporated into the segmentation network for the implementation of prototype generation and contrastive learning, without altering the inherent training procedure of the model. The combined framework is evaluated on the classic setting of PASCAL VOC 2012, as shown in Table 7. It is clear that the combined framework achieves consistent performance gains over FixMatch, demonstrating the remarkable generalization of our approach. It is worth mentioning that further improvements may be attainable through fine-tuning of hyperparameters, since minor adjustments are made in our experiments.

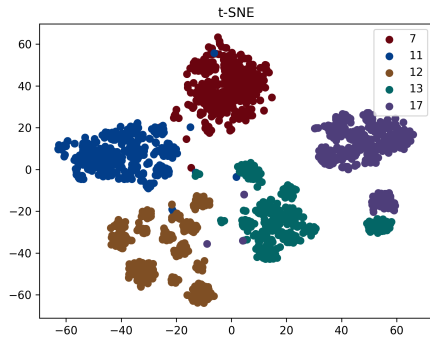
4.5. Qualitative Analysis

In this section, qualitative analyses are performed to illustrate the impact of our approach in the feature space and visualize the segmentation performance, thereby further validating its effectiveness.

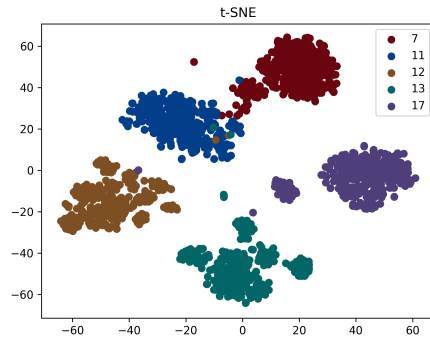
Distribution of feature representation. The core idea of our method is to generate prototypes that refine classification boundaries in the feature space. Thus, it is crucial to explore the influence of our approach on feature distributions. Fig. 5 shows the feature distributions of various methods for some categories in PASCAL VOC 2012. It can be observed that the feature distributions of each class generated by the models of “Plain L_{pro} ” and “Ours” are more compact than other methods, which aligns with the objective of prototype-based methods. However, the prototype distributions exhibit significant differences between the two methods.

As shown in Fig. 5 (c), multiple prototypes from different categories are clustered within the small “conflict” region (highlighted in the yellow circle), along with a number of challenging samples. This situation may potentially confuse the network in feature classification. In contrast, our method exhibits fewer “conflicts” in Fig. 5 (d), with the majority of prototypes located at the edges of feature distributions, indicating clear class boundaries. This corresponds to the superior performance of our model as reported in the quantitative results.

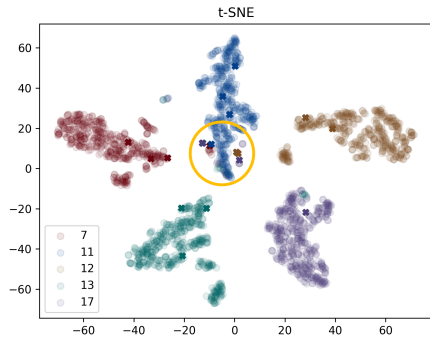
The different observations can be interpreted as follows: The prototypes initialized by “Plain L_{pro} ” tend to be closer to the semantic centers of the classes but further from the classification boundaries. This makes the network more vulnerable to the challenging samples, resulting in a relative un-



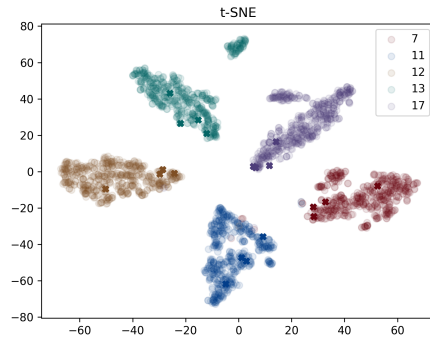
(a) SupOnly



(b) $L_{un\text{sup}}$



(c) Plain L_{pro}



(d) Ours w/ BRPG

Figure 5: t-SNE [75] visualization of feature distributions under 1/4 (366) partition of PASCAL VOC 2012. Models are trained with different settings: (a) SupOnly: Only supervised training. (b) $L_{un\text{sup}}$: Semi-supervised training with $L_{un\text{sup}}$. (c) Plain L_{pro} : Plain prototype-based contrastive learning framework with random sampling and direct K-Means clustering. (d) Ours w/ BRPG: Our training pipeline with BRPG. The corresponding relationship between the displayed ID and semantic category is: {7: “car”, 11: “diningtable”, 12: “dog”, 13: “horse”, 17: “sheep”}.

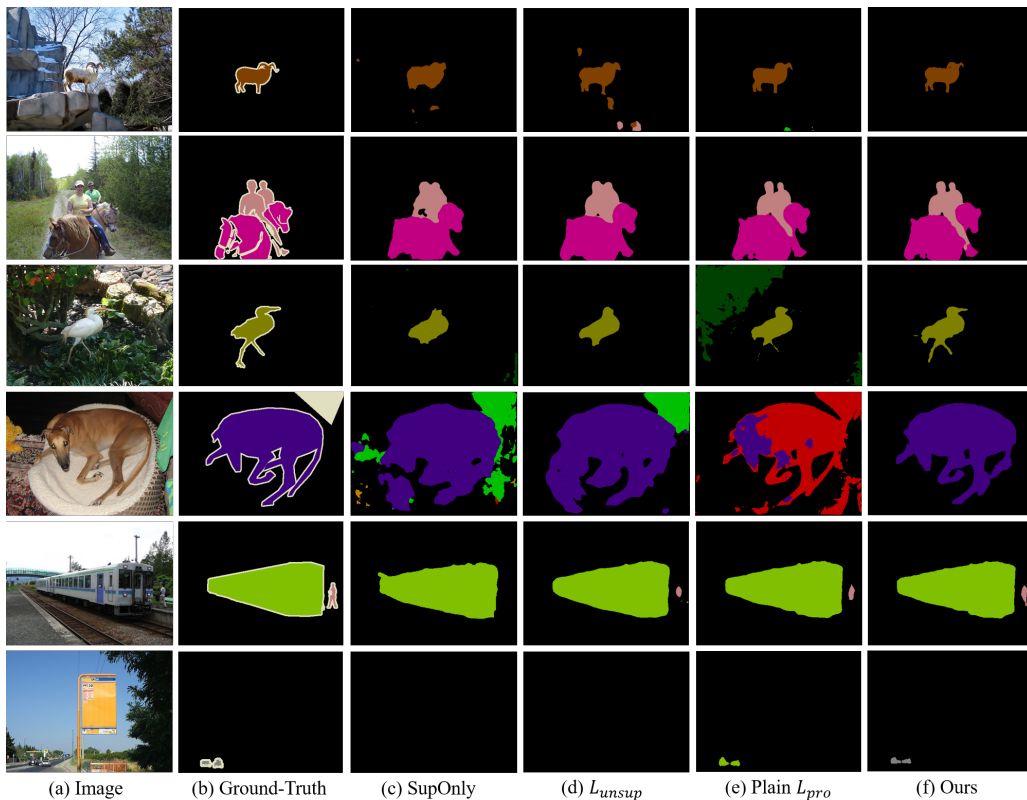


Figure 6: Qualitative results on the *classic* setting of **PASCAL VOC 2012** under 1/4 partition protocol. (a) Input images. (b) Ground-truth. (c) Supervised-only model. (d) Semi-supervised model without prototype-based learning. (e) Plain prototype-based model. (f) Our proposed model with BRPG.

stable training process. The instability may negatively affect the feature generation and prototype update procedures. In contrast, our approach generates prototypes that are closer to the classification boundaries, which alleviates the negative impact of challenging samples and leads to a more stable training process. Consequently, the proposed method achieves more favorable feature and prototype distributions.

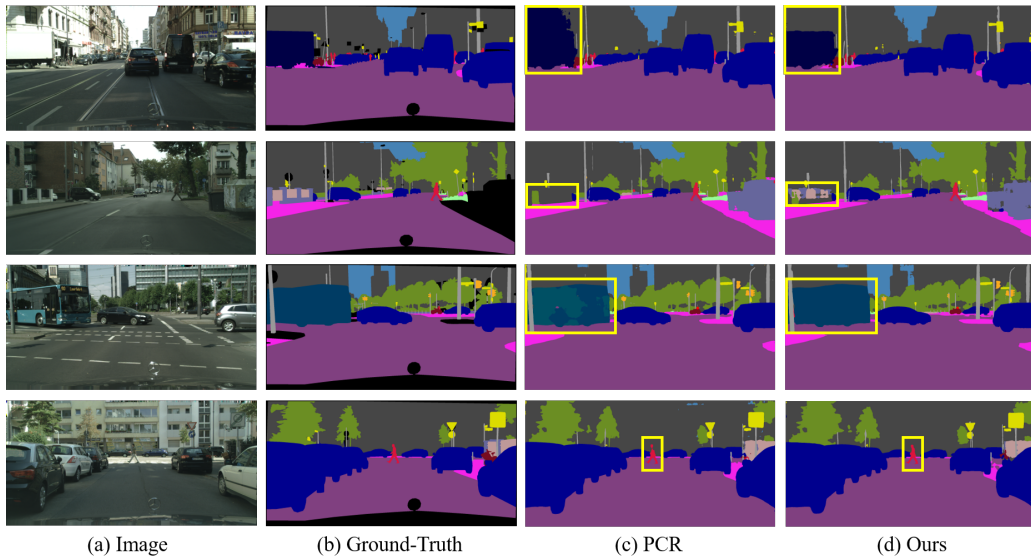


Figure 7: Qualitative results on **Cityscapes** under 1/16 partition protocol. (a) Input images. (b) Ground-truth. (c) the SOTA prototype-based method PCR. (d) Our method. Yellow rectangles highlight the promotion of segmentation results by our approach.

Qualitative results on different components. Fig. 6 presents the qualitative results when using different components of the proposed approach. It can be seen that the SupOnly model (c) is prone to yield incomplete and noisy predictions, whereas the semi-supervised model (d) produces more robust segments. The prototype-based method (e) effectively refines the object boundaries with a superior perception of class semantics. However, it may introduce noise (row 3) and exhibit misclassifications (row 4) in scenarios with cluttered backgrounds. In contrast, our method (f) generates finer object boundaries and demonstrates cleaner and more accurate predictions compared to (e). Furthermore, superior performance can be achieved in small object segmentation tasks (row 5 and row 6) with our approach. These

visualization results further support the effectiveness of BRPG in perceiving category boundaries.

Qualitative results on relevant methods. In the qualitative comparison results on Cityscapes (Fig. 7), our method outperforms the prototype-based method PCR [28] in several aspects: (1) Enhanced accuracy in predicting challenging object boundaries. For instance, in the first row, our method successfully distinguishes between the white truck and the white building. (2) Increased capability to identify additional object classes, e.g., the fence and wall highlighted in the second row. (3) Improved semantic consistency within objects, shown in the third row where our approach achieves consistent category predictions within the bus, while the comparison method predicts different categories within the same object. (4) Superior edge details in object predictions, such as the person highlighted in the fourth row. These findings demonstrate the superiority of the proposed method as a prototype-based approach.

5. Conclusion

In this paper, a novel end-to-end prototype-based approach for semi-supervised semantic segmentation is proposed, which improves the segmentation performance through boundary-refined prototype generation (BRPG). Specifically, we investigate the relationship between feature distributions and predicted confidence, and propose the confidence-based prototype generation (CPG) method. CPG categorizes extracted features into high-confidence and low-confidence groups using a threshold, followed by online sampling and clustering. This operation allows the low-confidence prototypes to be

closer to the initial classification boundaries. Besides, an adaptive prototype optimization (APO) method is introduced to increase the number of cluster centers for categories with scattered feature distributions, further refining the class boundaries. The initialized prototypes are then utilized to guide the contrastive learning during model training. Experimental results on benchmark datasets demonstrate that our proposed method outperforms the existing state-of-the-art methods. Furthermore, extensive ablation studies confirm the robustness and reliability of the proposed approach, and the compatibility with FixMatch serves as strong evidence for its generalization capability. Finally, qualitative results provide the visual proofs for its effectiveness, especially in object boundary perception.

In future work, an optimal sampling strategy based on class-specific confidence thresholding will be further explored, as discussed in Section 4.3. Moreover, considering the imbalanced class distributions in the datasets, it is required to explore more class-specific methods throughout the entire framework. We also believe that the proposed method can tackle weakly-supervised problems, which we intend to explore in the future.

References

- [1] D. Feng, C. Haase-Schütz, L. Rosenbaum, H. Hertlein, C. Glaeser, F. Timm, W. Wiesbeck, K. Dietmayer, Deep multi-modal object detection and semantic segmentation for autonomous driving: Datasets, methods, and challenges, *IEEE Transactions on Intelligent Transportation Systems* 22 (2020) 1341–1360.
- [2] M. Siam, M. Gamal, M. Abdel-Razek, S. Yogamani, M. Jagersand,

- H. Zhang, A comparative study of real-time semantic segmentation for autonomous driving, in: Proceedings of the IEEE conference on computer vision and pattern recognition workshops, 2018, pp. 587–597.
- [3] S. Asgari Taghanaki, K. Abhishek, J. P. Cohen, J. Cohen-Adad, G. Hamarneh, Deep semantic segmentation of natural and medical images: a review, *Artificial Intelligence Review* 54 (2021) 137–178.
- [4] L.-C. Chen, G. Papandreou, I. Kokkinos, K. Murphy, A. L. Yuille, Deeplab: Semantic image segmentation with deep convolutional nets, atrous convolution, and fully connected crfs, *IEEE transactions on pattern analysis and machine intelligence* 40 (2017) 834–848.
- [5] J. Long, E. Shelhamer, T. Darrell, Fully convolutional networks for semantic segmentation, in: Proceedings of the IEEE conference on computer vision and pattern recognition, 2015, pp. 3431–3440.
- [6] O. Ronneberger, P. Fischer, T. Brox, U-net: Convolutional networks for biomedical image segmentation, in: *Medical Image Computing and Computer-Assisted Intervention–MICCAI 2015: 18th International Conference, Munich, Germany, October 5-9, 2015, Proceedings, Part III* 18, Springer, 2015, pp. 234–241.
- [7] H. Zhao, J. Shi, X. Qi, X. Wang, J. Jia, Pyramid scene parsing network, in: Proceedings of the IEEE conference on computer vision and pattern recognition, 2017, pp. 2881–2890.
- [8] Z. Wang, Z. Zhao, X. Xing, D. Xu, X. Kong, L. Zhou, Conflict-based cross-view consistency for semi-supervised semantic segmentation, in:

Proceedings of the IEEE/CVF Conference on Computer Vision and Pattern Recognition, 2023, pp. 19585–19595.

- [9] X. Chen, Y. Yuan, G. Zeng, J. Wang, Semi-supervised semantic segmentation with cross pseudo supervision, in: Proceedings of the IEEE/CVF Conference on Computer Vision and Pattern Recognition, 2021, pp. 2613–2622.
- [10] X. Wang, B. Zhang, L. Yu, J. Xiao, Hunting sparsity: Density-guided contrastive learning for semi-supervised semantic segmentation, in: Proceedings of the IEEE/CVF Conference on Computer Vision and Pattern Recognition, 2023, pp. 3114–3123.
- [11] I. Alonso, A. Sabater, D. Ferstl, L. Montesano, A. C. Murillo, Semi-supervised semantic segmentation with pixel-level contrastive learning from a class-wise memory bank, in: Proceedings of the IEEE/CVF International Conference on Computer Vision, 2021, pp. 8219–8228.
- [12] H. Chen, Y. Jin, G. Jin, C. Zhu, E. Chen, Semisupervised semantic segmentation by improving prediction confidence, *IEEE Transactions on Neural Networks and Learning Systems* 33 (2021) 4991–5003.
- [13] G. French, S. Laine, T. Aila, M. Mackiewicz, G. Finlayson, Semi-supervised semantic segmentation needs strong, varied perturbations, *arXiv preprint arXiv:1906.01916* (2019).
- [14] Y. Wang, H. Wang, Y. Shen, J. Fei, W. Li, G. Jin, L. Wu, R. Zhao, X. Le, Semi-supervised semantic segmentation using unreliable pseudo-labels,

- in: Proceedings of the IEEE/CVF Conference on Computer Vision and Pattern Recognition, 2022, pp. 4248–4257.
- [15] W.-C. Hung, Y.-H. Tsai, Y.-T. Liou, Y.-Y. Lin, M.-H. Yang, Adversarial learning for semi-supervised semantic segmentation, arXiv preprint arXiv:1802.07934 (2018).
- [16] N. Souly, C. Spampinato, M. Shah, Semi supervised semantic segmentation using generative adversarial network, in: Proceedings of the IEEE international conference on computer vision, 2017, pp. 5688–5696.
- [17] S. Mittal, M. Tatarchenko, T. Brox, Semi-supervised semantic segmentation with high-and low-level consistency, IEEE transactions on pattern analysis and machine intelligence 43 (2019) 1369–1379.
- [18] Y. Ouali, C. Hudelot, M. Tami, Semi-supervised semantic segmentation with cross-consistency training, in: Proceedings of the IEEE/CVF Conference on Computer Vision and Pattern Recognition, 2020, pp. 12674–12684.
- [19] Y. Liu, Y. Tian, Y. Chen, F. Liu, V. Belagiannis, G. Carneiro, Perturbed and strict mean teachers for semi-supervised semantic segmentation, in: Proceedings of the IEEE/CVF Conference on Computer Vision and Pattern Recognition, 2022, pp. 4258–4267.
- [20] Y. Zou, Z. Zhang, H. Zhang, C.-L. Li, X. Bian, J.-B. Huang, T. Pfister, Pseudoseg: Designing pseudo labels for semantic segmentation, arXiv preprint arXiv:2010.09713 (2020).

- [21] D. Kwon, S. Kwak, Semi-supervised semantic segmentation with error localization network, in: Proceedings of the IEEE/CVF Conference on Computer Vision and Pattern Recognition, 2022, pp. 9957–9967.
- [22] R. Mendel, L. A. De Souza, D. Rauber, J. P. Papa, C. Palm, Semi-supervised segmentation based on error-correcting supervision, in: Computer Vision–ECCV 2020: 16th European Conference, Glasgow, UK, August 23–28, 2020, Proceedings, Part XXIX 16, Springer, 2020, pp. 141–157.
- [23] L. Yang, W. Zhuo, L. Qi, Y. Shi, Y. Gao, St++: Make self-training work better for semi-supervised semantic segmentation, in: Proceedings of the IEEE/CVF Conference on Computer Vision and Pattern Recognition, 2022, pp. 4268–4277.
- [24] X. Lai, Z. Tian, L. Jiang, S. Liu, H. Zhao, L. Wang, J. Jia, Semi-supervised semantic segmentation with directional context-aware consistency, in: Proceedings of the IEEE/CVF Conference on Computer Vision and Pattern Recognition, 2021, pp. 1205–1214.
- [25] Y. Zhong, B. Yuan, H. Wu, Z. Yuan, J. Peng, Y.-X. Wang, Pixel contrastive-consistent semi-supervised semantic segmentation, in: Proceedings of the IEEE/CVF International Conference on Computer Vision, 2021, pp. 7273–7282.
- [26] S. Liu, S. Zhi, E. Johns, A. J. Davison, Bootstrapping semantic segmentation with regional contrast, arXiv preprint arXiv:2104.04465 (2021).

- [27] T. Zhou, W. Wang, E. Konukoglu, L. Van Gool, Rethinking semantic segmentation: A prototype view, in: Proceedings of the IEEE/CVF Conference on Computer Vision and Pattern Recognition, 2022, pp. 2582–2593.
- [28] H. Xu, L. Liu, Q. Bian, Z. Yang, Semi-supervised semantic segmentation with prototype-based consistency regularization, Advances in Neural Information Processing Systems 35 (2022) 26007–26020.
- [29] M. Everingham, L. Van Gool, C. K. Williams, J. Winn, A. Zisserman, The pascal visual object classes (voc) challenge, International journal of computer vision 88 (2010) 303–338.
- [30] Z. Dai, Z. Yang, F. Yang, W. W. Cohen, R. R. Salakhutdinov, Good semi-supervised learning that requires a bad gan, Advances in neural information processing systems 30 (2017).
- [31] A. Tarvainen, H. Valpola, Mean teachers are better role models: Weight-averaged consistency targets improve semi-supervised deep learning results, Advances in neural information processing systems 30 (2017).
- [32] M. Cordts, M. Omran, S. Ramos, T. Rehfeld, M. Enzweiler, R. Benenson, U. Franke, S. Roth, B. Schiele, The cityscapes dataset for semantic urban scene understanding, in: Proceedings of the IEEE conference on computer vision and pattern recognition, 2016, pp. 3213–3223.
- [33] K. Sohn, D. Berthelot, N. Carlini, Z. Zhang, H. Zhang, C. A. Raffel, E. D. Cubuk, A. Kurakin, C.-L. Li, Fixmatch: Simplifying semi-

- supervised learning with consistency and confidence, *Advances in neural information processing systems* 33 (2020) 596–608.
- [34] J. E. Van Engelen, H. H. Hoos, A survey on semi-supervised learning, *Machine learning* 109 (2020) 373–440.
- [35] S. Laine, T. Aila, Temporal ensembling for semi-supervised learning, *arXiv preprint arXiv:1610.02242* (2016).
- [36] D. Berthelot, N. Carlini, I. Goodfellow, N. Papernot, A. Oliver, C. A. Raffel, Mixmatch: A holistic approach to semi-supervised learning, *Advances in neural information processing systems* 32 (2019).
- [37] V. Verma, K. Kawaguchi, A. Lamb, J. Kannala, A. Solin, Y. Bengio, D. Lopez-Paz, Interpolation consistency training for semi-supervised learning, *Neural Networks* 145 (2022) 90–106.
- [38] Q. Xie, Z. Dai, E. Hovy, T. Luong, Q. Le, Unsupervised data augmentation for consistency training, *Advances in neural information processing systems* 33 (2020) 6256–6268.
- [39] T. Miyato, S.-i. Maeda, M. Koyama, K. Nakae, S. Ishii, Distributional smoothing with virtual adversarial training, *arXiv preprint arXiv:1507.00677* (2015).
- [40] D.-H. Lee, et al., Pseudo-label: The simple and efficient semi-supervised learning method for deep neural networks, in: *Workshop on challenges in representation learning, ICML*, volume 3, Atlanta, 2013, p. 896.

- [41] Y. Chen, X. Zhu, S. Gong, Semi-supervised deep learning with memory, in: Proceedings of the European conference on computer vision (ECCV), 2018, pp. 268–283.
- [42] P. Cascante-Bonilla, F. Tan, Y. Qi, V. Ordonez, Curriculum labeling: Revisiting pseudo-labeling for semi-supervised learning, in: Proceedings of the AAAI conference on artificial intelligence, volume 35, 2021, pp. 6912–6920.
- [43] T. N. Kipf, M. Welling, Semi-supervised classification with graph convolutional networks, arXiv preprint arXiv:1609.02907 (2016).
- [44] A. Iscen, G. Tolias, Y. Avrithis, O. Chum, Label propagation for deep semi-supervised learning, in: Proceedings of the IEEE/CVF conference on computer vision and pattern recognition, 2019, pp. 5070–5079.
- [45] D. P. Kingma, S. Mohamed, D. Jimenez Rezende, M. Welling, Semi-supervised learning with deep generative models, Advances in neural information processing systems 27 (2014).
- [46] L. Maaløe, C. K. Sønderby, S. K. Sønderby, O. Winther, Auxiliary deep generative models, in: International conference on machine learning, PMLR, 2016, pp. 1445–1453.
- [47] G.-J. Qi, L. Zhang, H. Hu, M. Edraki, J. Wang, X.-S. Hua, Global versus localized generative adversarial nets, in: Proceedings of the IEEE conference on computer vision and pattern recognition, 2018, pp. 1517–1525.

- [48] X. Zhai, A. Oliver, A. Kolesnikov, L. Beyler, S4l: Self-supervised semi-supervised learning, in: Proceedings of the IEEE/CVF international conference on computer vision, 2019, pp. 1476–1485.
- [49] T. Chen, S. Kornblith, M. Norouzi, G. Hinton, A simple framework for contrastive learning of visual representations, in: International conference on machine learning, PMLR, 2020, pp. 1597–1607.
- [50] T. Chen, S. Kornblith, K. Swersky, M. Norouzi, G. E. Hinton, Big self-supervised models are strong semi-supervised learners, *Advances in neural information processing systems* 33 (2020) 22243–22255.
- [51] L. Yang, L. Qi, L. Feng, W. Zhang, Y. Shi, Revisiting weak-to-strong consistency in semi-supervised semantic segmentation, in: Proceedings of the IEEE/CVF Conference on Computer Vision and Pattern Recognition, 2023, pp. 7236–7246.
- [52] Z. Ke, D. Qiu, K. Li, Q. Yan, R. W. Lau, Guided collaborative training for pixel-wise semi-supervised learning, in: *Computer Vision–ECCV 2020: 16th European Conference, Glasgow, UK, August 23–28, 2020, Proceedings, Part XIII 16*, Springer, 2020, pp. 429–445.
- [53] R. He, J. Yang, X. Qi, Re-distributing biased pseudo labels for semi-supervised semantic segmentation: A baseline investigation, in: Proceedings of the IEEE/CVF International Conference on Computer Vision, 2021, pp. 6930–6940.
- [54] H. Hu, F. Wei, H. Hu, Q. Ye, J. Cui, L. Wang, Semi-supervised semantic

- segmentation via adaptive equalization learning, *Advances in Neural Information Processing Systems* 34 (2021) 22106–22118.
- [55] D. Guan, J. Huang, A. Xiao, S. Lu, Unbiased subclass regularization for semi-supervised semantic segmentation, in: *Proceedings of the IEEE/CVF Conference on Computer Vision and Pattern Recognition*, 2022, pp. 9968–9978.
- [56] H. Xie, C. Wang, M. Zheng, M. Dong, S. You, C. Fu, C. Xu, Boosting semi-supervised semantic segmentation with probabilistic representations, in: *Proceedings of the AAAI Conference on Artificial Intelligence*, volume 37, 2023, pp. 2938–2946.
- [57] R. O. Duda, P. E. Hart, et al., *Pattern classification and scene analysis*, volume 3, Wiley New York, 1973.
- [58] T. Hastie, R. Tibshirani, J. H. Friedman, J. H. Friedman, *The elements of statistical learning: data mining, inference, and prediction*, volume 2, Springer, 2009.
- [59] T. Cover, P. Hart, Nearest neighbor pattern classification, *IEEE transactions on information theory* 13 (1967) 21–27.
- [60] B. J. Knowlton, L. R. Squire, The learning of categories: Parallel brain systems for item memory and category knowledge, *Science* 262 (1993) 1747–1749.
- [61] E. H. Rosch, Natural categories, *Cognitive psychology* 4 (1973) 328–350.

- [62] N. Dong, E. P. Xing, Few-shot semantic segmentation with prototype learning., in: BMVC, volume 3, 2018.
- [63] O. Vinyals, C. Blundell, T. Lillicrap, D. Wierstra, et al., Matching networks for one shot learning, *Advances in neural information processing systems* 29 (2016).
- [64] K. Wang, J. H. Liew, Y. Zou, D. Zhou, J. Feng, Panet: Few-shot image semantic segmentation with prototype alignment, in: *proceedings of the IEEE/CVF international conference on computer vision*, 2019, pp. 9197–9206.
- [65] B. Hariharan, P. Arbeláez, L. Bourdev, S. Maji, J. Malik, Semantic contours from inverse detectors, in: *2011 international conference on computer vision*, IEEE, 2011, pp. 991–998.
- [66] K. He, X. Zhang, S. Ren, J. Sun, Deep residual learning for image recognition, in: *Proceedings of the IEEE conference on computer vision and pattern recognition*, 2016, pp. 770–778.
- [67] J. Deng, W. Dong, R. Socher, L.-J. Li, K. Li, L. Fei-Fei, Imagenet: A large-scale hierarchical image database, in: *2009 IEEE conference on computer vision and pattern recognition*, Ieee, 2009, pp. 248–255.
- [68] L.-C. Chen, Y. Zhu, G. Papandreou, F. Schroff, H. Adam, Encoder-decoder with atrous separable convolution for semantic image segmentation, in: *Proceedings of the European conference on computer vision (ECCV)*, 2018, pp. 801–818.

- [69] P. Micikevicius, S. Narang, J. Alben, G. Diamos, E. Elsen, D. Garcia, B. Ginsburg, M. Houston, O. Kuchaiev, G. Venkatesh, et al., Mixed precision training, arXiv preprint arXiv:1710.03740 (2017).
- [70] Y. Jin, J. Wang, D. Lin, Semi-supervised semantic segmentation via gentle teaching assistant, *Advances in Neural Information Processing Systems* 35 (2022) 2803–2816.
- [71] P. Qiao, Z. Wei, Y. Wang, Z. Wang, G. Song, F. Xu, X. Ji, C. Liu, J. Chen, Fuzzy positive learning for semi-supervised semantic segmentation, in: *Proceedings of the IEEE/CVF Conference on Computer Vision and Pattern Recognition*, 2023, pp. 15465–15474.
- [72] Y. Lin, H. Xu, L. Liu, J. Zou, J. Q. Shi, Revisiting image reconstruction for semi-supervised semantic segmentation, arXiv preprint arXiv:2303.09794 (2023).
- [73] L. Wu, L. Fang, X. He, M. He, J. Ma, Z. Zhong, Querying labeled for unlabeled: Cross-image semantic consistency guided semi-supervised semantic segmentation, *IEEE Transactions on Pattern Analysis and Machine Intelligence* (2023).
- [74] R. Chen, T. Chen, Q. Wang, Y. Yao, Semi-supervised semantic segmentation with region relevance, arXiv preprint arXiv:2304.11539 (2023).
- [75] L. Van der Maaten, G. Hinton, Visualizing data using t-sne., *Journal of machine learning research* 9 (2008).